Image processing on meso-scale photographs of brittle shear zones

Poorvi Hebbar[1], Soumyajit Mukherjee[2]*, Narayan Bose[2]

1. Department of Computer Science and Engineering, Indian Institute of Technology Bombay, Powai, Mumbai 400 076, Maharashtra, INDIA

2. Department of Earth Sciences, Indian Institute of Technology Bombay, Powai, Mumbai 400 076, Maharashtra, INDIA

***Author for correspondence:** smoumyajitm@gmail.com, smukherjee@iitb.ac.in

Abstract

Study of structures and fabrics from different scales of observation is an indispensible first step in structural geology. We process three selected images of brittle shear zones using various methods, steps and filters. Such an exercise is more effective to detect brittle planes when the planes are not too close-spaced and is devoid of white fault gouge. Edge detection methods using fuzzy logic seems to be one of the best methods to detect shear planes more distinctly. Notwithstanding, a structural geologists's first identification and categorization of structures in the field or in other scales continues to be indispensible.

Words: 98

Keywords: Image interpretation; cracks; joints; mathematical method; shear sense; shear zone

Highlights:

I. Image processing techniques applied to brittle shear zones photographs, to enhance images
II. Discussion made on usefulness of such exercise in better identification of shear planes

1. Introduction

Correct geological interpretation of structures documented in field or from other scales of observations **(Mukherjee 2021)** has been of paramount importance in structural geology. Field-sketches were done profusely by the field geologists (**Genge 2020**) before cameras became handy. Subsequently, with the advent of digital cameras and smart phones **(Novakova and Pavlis 2017)**, photography and other structural geological activities in the field became quite easy. Having a huge space in the electronic device, geologists now take numerous photographs of geological structures. However, after getting back from field, one may note that not all photographs are of good quality, or in few images a very detail of structures are required to be presented. In such cases, geological snaps can be required to undertake image processing. However, if the primary image is poor, chances are that image analysis can help to recover features with a limit (**Heilbronner and Barrett 2014**). One of the main outcomes of image analysis in structural geology is to enhance the geological feature of key interest **(Bjørnerud and Boyer 1996)** in an unbiased, reproducible, quantitative and time-saving way (**Bons and Jessell 1996**).

In applied structural geological contexts, images have been processed for seismic (**Misra and Mukherjee 2018**), boreholes **(e.g., Cornet 2013)**, microstructures **(e.g., Mokhles *et al.* 2019)**, remote sensing **(e.g., Sulaksana and Hamdani 2014)** etc. Matlab programme has recently been developed to study fracture patters (**Healy *et al.* 2017**). Image analyses if done carefully can produce a good number of following outcomes (**Bjørnerud and Boyer 1996**) calculation of object areas, perimeters/lengths, color/grayscale magnitudes, and for lenticular objects- axial lengths, orientations, *x-y* centers, point-counting, strain analysis, areal estimation, and assessment of lattice and grain-shape preferred orientation.

This work applies several standard image processing methods on structural geological images take from meso-scale. We finally compare different methods/techniques and comment on the practice to get the best possible interpretation of geological photographs.

2. This work

Three images (**Figs. 1a, 2a, 3a**) of brittle shear zones with Y- and P-planes developed in different degrees were processed by standard techniques. These photographs were captured using a *Canon PowerShot SX150 IS* digital camera, and they come from the Inner Lesser Himalaya along the Bhagirathi river section, Uttarakhand, western Himalaya, India. Low-grade meta-sedimentary rocks, mostly quartzites (**Fig. 1a**), limestones (**Figs. 2a, 3a**) and schists are present along this traverse. Detail of structural geology of the location can be found in **Bose *et al.* (2018)** and **Bose and Mukherjee (2019)**. Sigmoid P-planes are bound by Y-planes were found from these images in naked eyes, and in the field a top-to-N/NE back-shear is indicated. The timing of this specific deformation from this Himalayan section has remained unknown till date.

While interpreting, figures have been named as *"Xyz"* in both main text as well as in **Repository 1**. Here *X* stands for the methods applied, *y* denotes figure number (*a* for **Fig. 1a**, *b* for **Fig. 2a** and *c* for **Fig. 3a**), and *z* represents steps used in the applied methods (**Table 1**). For example, *Abc* will mean image segmentation applied on image *b* with RGB to greyscale step involved. Matlab programs were written for each of the image enhancement process **(Repository 1)**. The image analyses did not have any preferred choice for some specific fractures. For example, the grain boundaries were also enhanced along with the brittle P- and Y-planes. **Repository 2** presents altogether 61 interpreted images, with about 20 each from the given 3 uninterpreted images. In Section-3 "Discussions", we present few key images in order to compare the output.

[Insert Table 1 about here]

3. Discussions

In the image segmentation method (method *A*), no significant differences are found amongst the uninterpreted image (**Fig. 1a**), the contrast stretched image (**Fig. 1b**), and the greyscale image **(Fig. 1c)**. No significant improvement is found also for fuzzy logic image processing (method *B*) when the RGB to greyscale conversion was made (image *Bab* in **Repository 2**). However, in case of the segmented crack approach under method *B*, curvature of the P-plane is clearly visible near the middle part of the image **(Fig. 1d)**. The cleaned image **(Fig. 1e)** under method *B* shows fractures with equal ease as that of the **Fig. 1d.** When Fuzzy logic image processing (method *B*) with I_X: gradient of intensities is applied, shear zones take an appearance **(Fig. 1f)**, which perhaps only a structural geologist who has seen the field exposure **(Fig. 1a)** earlier can interpret. However, when Fuzzy logic image processing (method *B*) with I_y: gradient of intensities is applied, the shear planes are not at all decipherable (image *Bad* in **Repository 2**), even though we have a prior idea about the original uninterpreted image (**Fig. 1a**). One of the best manifestations of P and Y planes appear when edge detection using fuzzy logic is applied (**Fig.**

1g). In this case, the right portion of the image demonstrates both the P and the Y planes quite distinctly. When bilateral filtering (method *C*) is done and different steps applied, there is no significant improvement in identifying the brittle planes Y and P in the obtained images (image *Caa* up to *Cae* in **Repository 2**) when compared with the uninterpretd image (**Fig. 1a**). The LoG (image *Dag* in **Repository 2**) and the zerocross (image *Dah* in **Repository 2**) processes yield clumsy output and can be more difficult to identify the planes Y and P, than the simple uninterpreted image (**Fig. 1a**). The Prewitt filter **(Fig. 1h)** and the Roberts filter **(Fig. 1i)** filter give better and cleaner images.

[Insert Figs. 1a-i about here]

Interestingly, when we apply image the segmentation method (method *A*) over another uninterpreted image (**Fig. 2a**), segmented crack (image *Abd* in **Repository 2**) and cleaned images (image *abe* in **Repository 2**) are impossible to decipher for Y and P planes and the shear sense. All the approaches of fuzzy logic image processing (method B) applied on **Fig. 2a** gives unsatisfactory images (images *Bba* to *Bbf* in **Repository 2**) that cannot be interpreted for Y and P planes. The same is true for the resultant images (images *Cba* to *Cbe*) in **Repository 2**) when bilateral filtering method is applied on **Fig. 2a.** Comparison between various fracture detection filter techniques (method D) when applied on **Fig. 2a,** LoG (image *Dbg* in **Repository 2**) and Zerocross filters (image *Dbh* in **Repository 2**) give the worst results. The Sobel filter here can produce an image where few of the shear planes are visible **(Fig. 2b)**, but still difficult to interpret than the simple visual interpretation of **Fig. 2a.**

[Insert Figs. 2a-b about here]

In case of the field photograph **Fig. 3a**, following the image segmentation method (method *A*) the segmented crack and the cleaned crack filters give white patches at the place where P- and Y planes are found otherwise. In Fuzzy logic image processing (method *B*), only the edge detection technique reveals P and Y planes somewhat clearly **(Fig. 3b)**. The same problem persists in all the output images (images *Dca* to *Dch* in **Repository 2**) in using the method of comparison between various fracture detection filter techniques (method *D*). In bilateral filtering method (method *C*), none of the output images (images *Cca* to *Cce* in **Repository 2**) give clear-cut P and Y planes.

[Insert Figs. 3a-b about here]

The main difference between the two field snaps **Figs. 1a** and **2a** is that in the later, the P-planes are more closely spaced than the former one. Possibly because of this, **Fig. 1a** after image processing, gave more distinct appearance of P and Y planes in few cases. **Fig. 3a** is a case with white fault gouge developed where P- and Y planes are found. Because of this white colour, many of the filtering approaches failed to pick up the Y and the P-planes, even though those are visible to the eyes of a trained structural geologist! For all the three starting images **Figs. 1a, 2a** and **3a,** their greyscale images deduced by various means do not significantly ease the detection of P and Y planes. In some of the methods, the thinned images and the zerocross images (e.g., images *Aaf* and *Dch*, respectively, in **Repository 2**) completely fail to bring out the Y and the P-planes.

4. Conclusions

A number of image enhancement methods, techniques and filters are available. Testing them on meso-scale photographs of brittle shear zones, led to understand the followings.

(i) One of the best manifestation of P and Y planes appear when edge detection using fuzzy logic is applied.

(ii) The zerocross and the thinned image techniques usually give poor ouput.

(iii) Greyscale images do not significantly enhance the photographs.

(iv) If the rock consists of white fine grained contents such as gouge material, image enhancement to detect brittle planes may not work well.

(v) Image enhancement on close-spaced planes possibly does not ease detection of those planes. For cases *(ii)* to *(v)*, a trained structural geologist's visual interpretation on field snaps can be more useful! In case, image processing also give ambiguous results, it will be better to undertake conventional thin-section studies of rocks to detect P and Y planes in microscale.

Acknowledgements: This work is a part of PH's research assignment for the course *GS 407: Structural Geology* taught by SM. CPDA grant (IIT Bombay) supported SM. **Chief Editor + Associate Editor + Managing Editor + Reviewers (+ proofreading team).**

Author credit statement:

PH: Programming and output images. **SM:** Supervision, manuscript writing. **NB:** Fieldwork, photography, commenting on the draft.

References

Bjørnerud M G and Boyer B. 1996 Image Analysis in Structural Geology Using NIH Image; In: *Structural Geology and Personal Computers* (ed.) De Paor D, Pergamon Press. Oxford. ISBN: 0 08 042430 9. pp. 105-122.

Bons P D and Jessell M 1996 Image Analysis in Structural Geology Using NIH Image; In: *Structural Geology and Personal Computers* (ed.) De Paor D, Pergamon Press. Oxford. ISBN: 0 08 042430 9. pp. 135-166.

Bose N, Dutta D and Mukherjee S 2018 Role of grain-size in phyllonitisation: Insights from mineralogy, microstructures, strain analyses and numerical modeling; *J. Struct. Geol.* **112** 39-52.

Bose N and Mukherjee S 2019 Field documentation and genesis of the back-structures from the Garhwal Lesser Himalaya, Uttarakhand, India. In: Crustal Architecture and Evolution of the Himalaya-Karakoram-Tibet Orogen. (eds) Sharma R, Villa I M and Kumar S, *Geol. Soc. London Spec. Publ.* **481** 111–125.

Genge M J 2020 *Geological Field Sketches and Illustrations: A Practical Guide*. Oxford University Press. ISBN 978–0–19–883592–9. pp. 1-293.

Healy D et al 2017 FracPaQ: A MATLAB™ toolbox for the quantification of fracture patterns; *J. Struct. Geol.* **95** 1-16.

Heilbronner R and Barrett S 2014 *Image Analysis in Earth Sciences: Microstructures and Textures of Earth Materials*. Springer-Verlag. Berlin. pp. 13. ISBN: 978-3-642-10342-1.

Internet ref: www.mathworks.com (Accessed on 25-May-2021)

Misra A A and Mukherjee S 2018 Seismic Structural Analysis. In: *Atlas of Structural Geological Interpretation from Seismic Images* (eds.) Misra A A, Mukherjee S, Wiley Blackwell. ISBN: 978-1-119-15832-5. pp. 15-26.

Mokhles M, Fatai A and Mohammed M 2019 *Advances in Rock Petrography: Image Processing Techniques for Automated Textural Thin Section Analysis*; Society of Petroleum Engineers. SPE-194835-MS.

Mukherjee S 2021 *Atlas of Structural Geology*. Second Edition. Elsevier. Amsterdam. ISBN: 978012816802. pp. 1-260.

Novakova L and Pavlis T L 2017 Assessment of the precision of smart phones and tablets for measurement of planar orientations: A case study; *J. Struct. Geol.* **97** 93-103.

Sulaksana N and Hamdani A M 2014 The Analysis of Remote Sensing Imagery for Predicting Structural Geology in Berau Basin East Kalimantan; *Int. J. Sci. Res.* 18-21. Article id: 020131349.

Fig. Captions

Fig. 1. See **Table 1** for the codes. **(a)** *Aaa;* **(b)** *Aab,* **(c)** *AAc* **(d)** *Aad,* **(e)** *Aae,* **(f)** *Aaf,* **(g)** *Baf,* **(h)** *Dae*, **(i)** *Daf*. Width of image ~ 3m. Berinag Formation. Quartzite exposed at 30.8136 °N, 78.6205 °E.

Fig. 2. See **Table 1** for the codes. **(a)** *Aba*, **(b)** *Dbc*. Width of image ~ 3m. Mandhali Formation. Limestone exposed at 30.6802°N, 78.3497°E.

Fig. 3. See **Table 1** for the codes. **(a)** *Aca*, **(b)** *Bcf*. Width of image ~ 1.5 m. Mandhali Formation. Limestone exposed at 30.6802°N, 78.3497°E.

Fig.a-d

Click here to access/download;Figure;Fig. 1_a-d.jpg

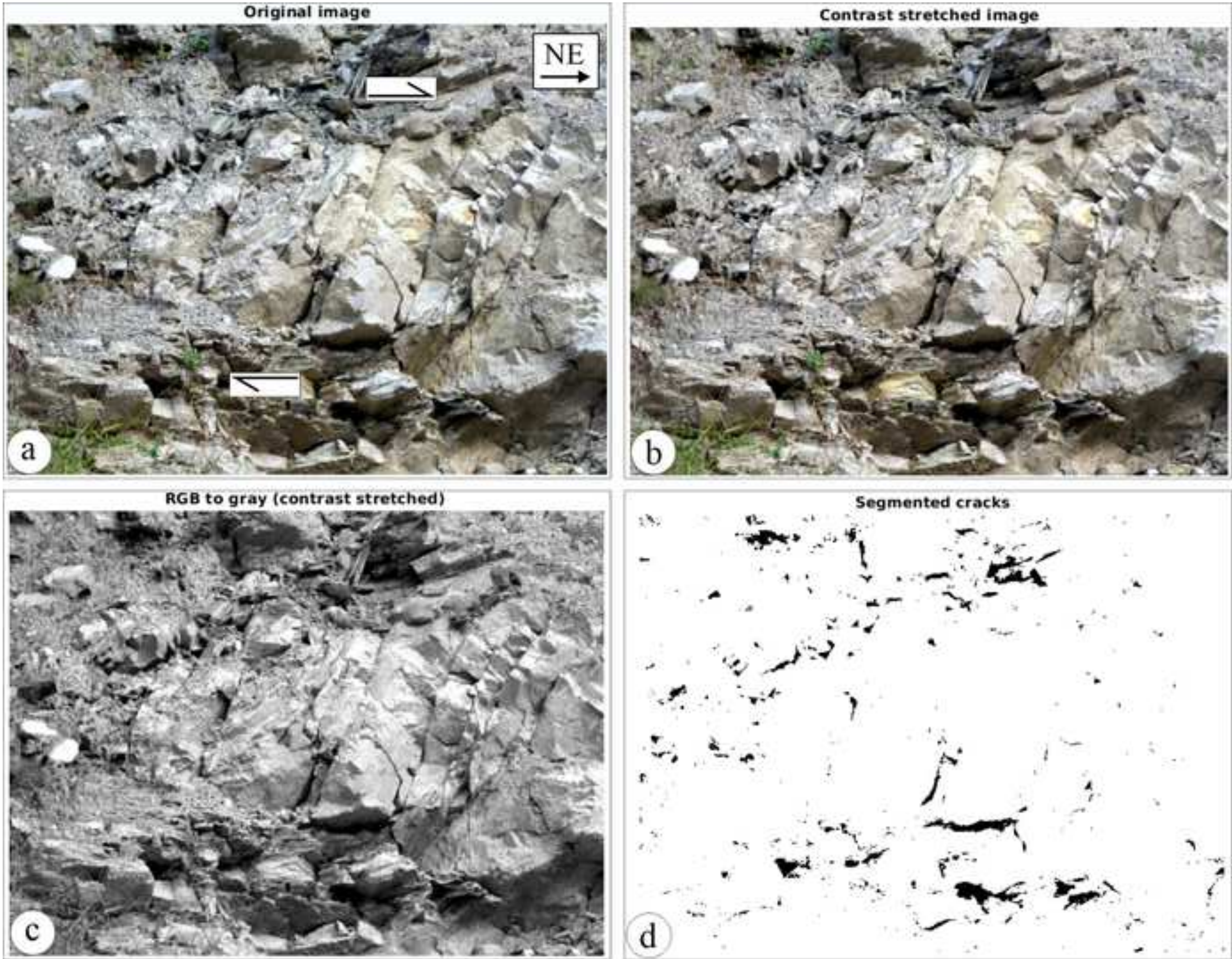

Fig. 1e-i

Click here to access/download;Figure;Fig. 1_e-i.jpg

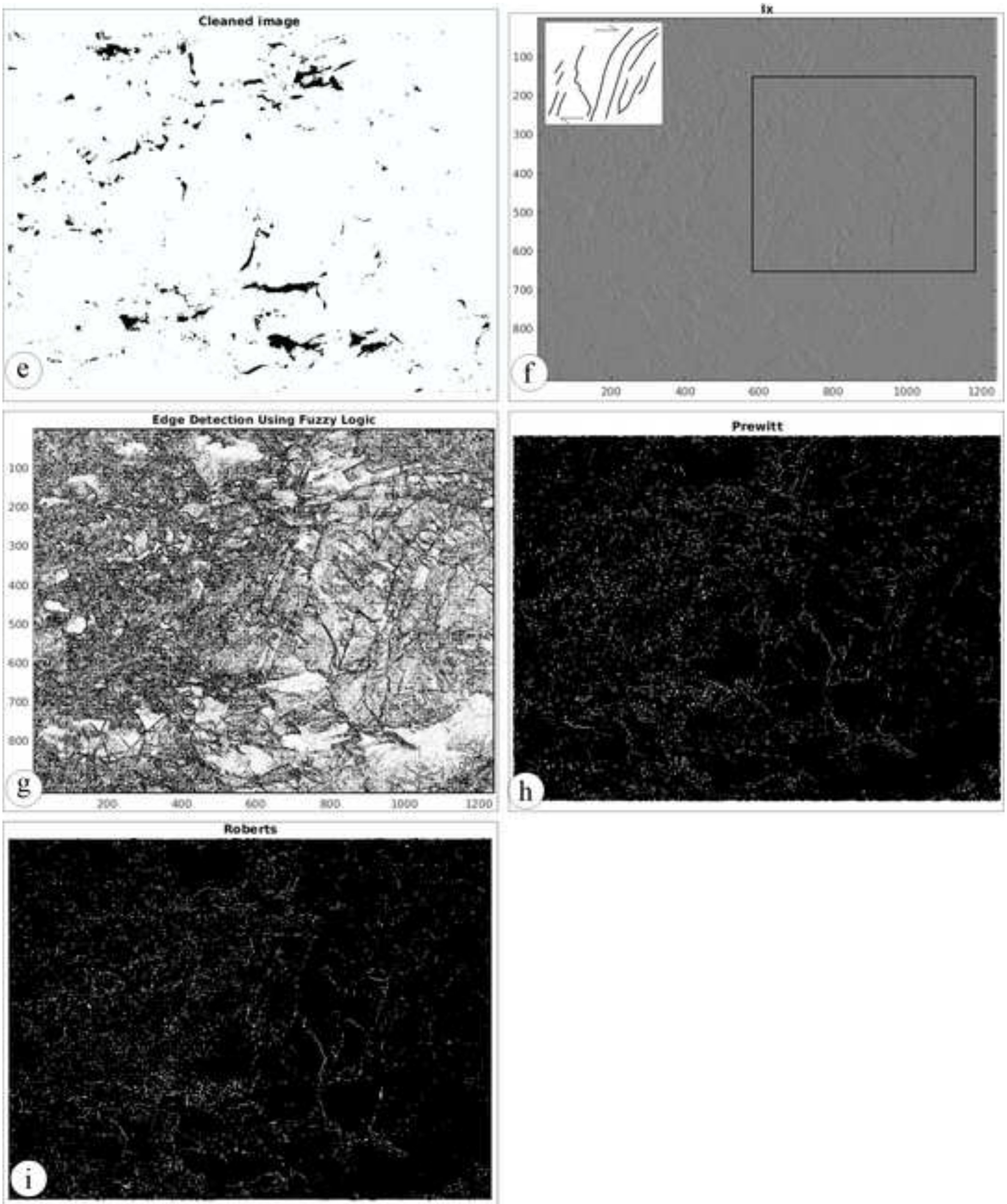

Fig. 2

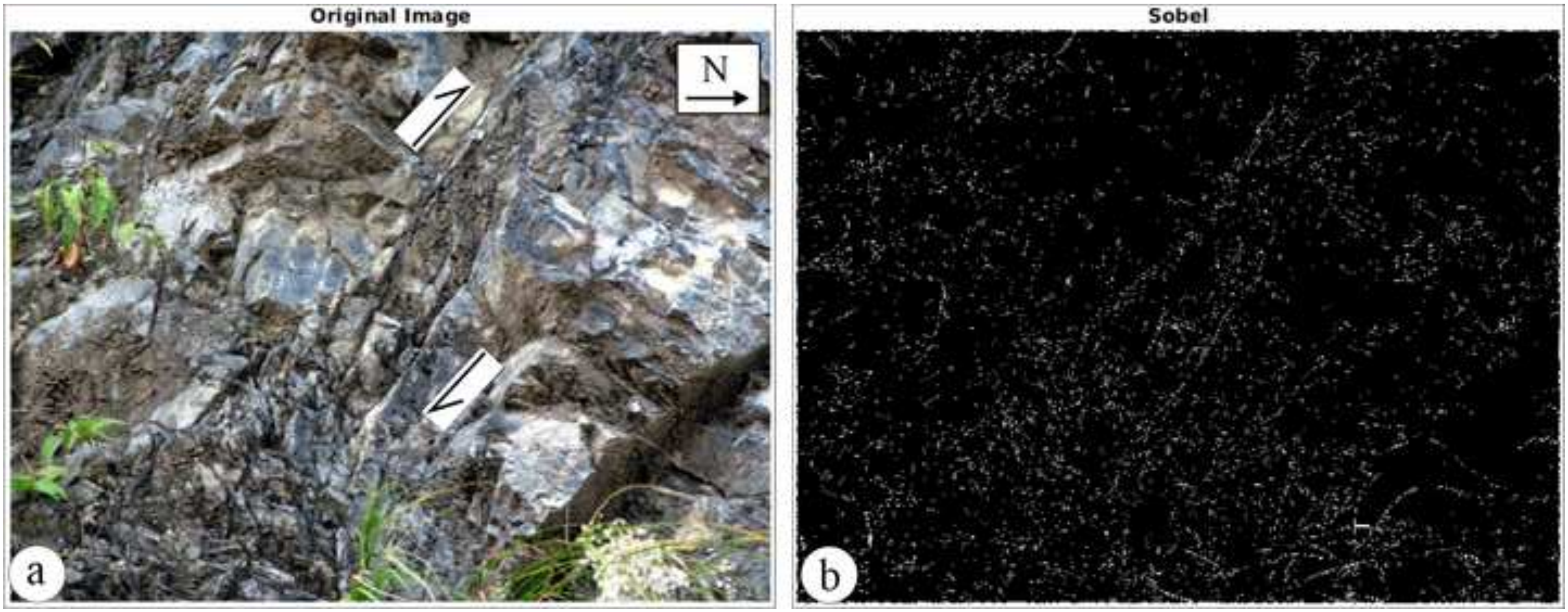

Fig. 3

Click here to access/download;Figure;Fig. 3(1).jpg

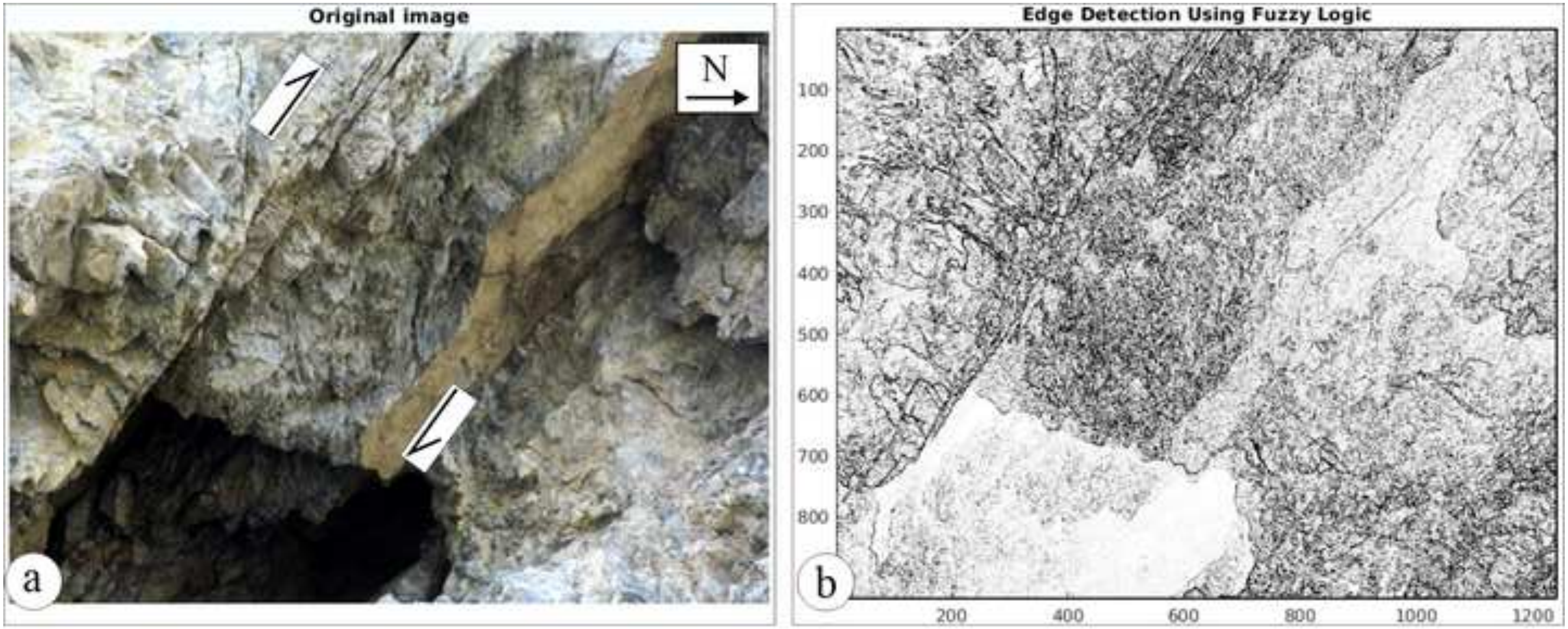

Table 1: Methods and Steps used in different methods.

X* in fig. code *Xyz	**Method**	***z* in fig. code *Xyz***	**Standard Approach** (Internet ref)
A	Image segmentation	a. Original uninterpreted image	
		b. Contrast stretched	Contrast is augmented in the image: Stretches the intensity range to span a desired range of magnitudes.
		c. RGB to greyscale	Alters RGB Images into gray scale. Average value of the three colors per pixel is taken.
		d. Segmented cracks	Alters the grayscale image into a binary image. Pixels in the input image are altered with a luminance more than a threshold level with the value 1 (white). Other pixels with the magnitude 0 (black).
		e. Cleaned image	Deletes isolated pixels (individual 1's surrounded by 0's or vice-versa).
		f. Thinned image	It removes pixels so that an object without holes shrinks to a minimally connected stroke, and an object with holes shrinks to a connected ring halfway between each hole and the outer boundary.
B	Fuzzy logic image processing	a. Original uninterpreted image	
		b. RGB to greyscale	See *A-c* above
		c. I_x: Gradient of intensities	Gradient of the intensities of image pixels along x-direction.
		d. I_y: Gradient of intensities	Gradient of the intensities of image pixels along y-direction.
		e. Degree of membership	A membership function is assigned with the specified type and parameters. Designates a zero-mean Gaussian membership function for each input. For gradient value for a pixel to be 0, it belongs to the zero membership function with a degree = 1. If sx and sy are the

			standard deviations for the zero membership function for the Ix and Iy inputs, for edge detector performance, theor magnitudes can be altered. Increasing the values renders the algorithm insensitive to the edges and reduces their intensity. Start, peak and end of the triangles of the membership functions can be altered to control the performance of the edge detector.
		f. Edge detection	Ix and Iy values can detect edges and mark as white pixels in the output Image. Pixel is colored white if it comes from a uniform region. It is black otherwise. A pixel is in a uniform region when the image gradient is zero along both the directions. One of these directions with a nonzero gradient means that then the pixel lies on an edge.
C	Bilateral filtering	a. Original uninterpreted image	
		b. RGB to greyscale	See *A-c* above.
		c. Binary gradient mask	Convert the grayscale image into binary image. This is achieved by replacing all pixels in the input image with luminance > a threshold level; value 1 (white) and replacing all other pixels 0 (black).
		d. Dilated gradient mask	Dilate the binary image, i.e., add pixels to the boundaries of objects in an image.
		e. Bilateral filtering	An edge preserving smoothing method, here a mask is made with weights for surrounding pixels and convolve it with the original image. The smoothed intensity at every pixel location x1 = weighted average of the surrounding pixels. The weight for a pixel location x2, for the intensity to be calculated at x1 is: *(i)* spatial distance between x1 and x2 (as the distance increases, weight reduces) *(ii)* dissimilarity between the intensity at x1 and x2 (higher the dissimilarity, reduced is the weight).
D	Comparison between various	a. Original uninterpreted image	
		b. RGB to greyscale	See *A-c* above

	fracture detection filter techniques	c. Sobel filter	Uses matrix mathematics to compute areas of different intensities of an image.
		d. Canny filter	Uses a multi-stage algorithm to detect a long range of edges in images.
		e. Prewitt filter	Uses a derivative mask and can detect only horizontal and vertical edges.
		f. Roberts filter	Performs a simple, quick, 2-D spatial gradient measurement. It works on a high spatial frequency region, often corresponding to edges. Matrices used: Gx=[[1 0] [0 -1]], Gy=[[0 1] [-1 0]].
		g. LoG filter	Finds edges by looking for zerocrossings after filtering with a Laplacian of Gaussian (LoG) filter.
		h. Zerocross filter	Finds edges by looking for zero-crossings.

Fig. Aae

Click here to access/download
Electronic Supplementary Material
Aae.png

Fig. Aaf

Fig. Aaa (Fig. 1a)

Click here to access/download
Electronic Supplementary Material
Fig. 1a_Aaa.png

Fig. Aab (Fig. 1b)

Fig. Aac (Fig. 1c)

Click here to access/download
Electronic Supplementary Material
Fig. 1c_Aac.png

Fig. Aad Fig. 1d)

Click here to access/download
Electronic Supplementary Material
Fig. 1d_Aad.png

Fig. Baa

Click here to access/download
Electronic Supplementary Material
Baa.png

Fig. Bab

Click here to access/download
Electronic Supplementary Material
Bab.png

Fig. Bad

Click here to access/download
Electronic Supplementary Material
Bad.png

Fig. Bae

Click here to access/download
Electronic Supplementary Material
Bae.png

Fig. Bac (Fig. 1f)

Click here to access/download
Electronic Supplementary Material
Fig. 1f_Bac.png

Fig. Baf (Fig. 1g)

Click here to access/download
Electronic Supplementary Material
Fig. 1g_Baf.png

Fig. Caa

Fig. Cab

Fig. Cac

Fig. Cad

Click here to access/download
Electronic Supplementary Material
Cad.png

Fig. Cae

Click here to access/download
Electronic Supplementary Material
Cae.png

Fig. Daa

Click here to access/download
Electronic Supplementary Material
Daa.png

Fig. Dab

Click here to access/download
Electronic Supplementary Material
Dab.png

Fig. Dac

Click here to access/download
Electronic Supplementary Material
Dac.png

Fig. Dad

Click here to access/download
Electronic Supplementary Material
Dad.png

Fig. Dag

Fig. Dah

Click here to access/download
Electronic Supplementary Material
Dah.png

Fig. Dae (Fig. 1h)

Click here to access/download

Electronic Supplementary Material

Fig. 1h_Dae.png

Fig. Daf (Fig. 1i)

Click here to access/download
Electronic Supplementary Material
Fig. 1i_Daf.png

Fig. Aba

Click here to access/download
Electronic Supplementary Material
Aba.png

Fig. Abb

Fig. Abc

Click here to access/download
Electronic Supplementary Material
Abc.png

Fig. Abd

Click here to access/download
Electronic Supplementary Material
Abd.png

Fig. Abe

Click here to access/download
Electronic Supplementary Material
Abe.png

Fig. Abf

Click here to access/download
Electronic Supplementary Material
Abf.png

Fig. Bba

Click here to access/download

Electronic Supplementary Material

Bba.png

Fig. Bbb

Fig. Bbc

Fig. Bbd

Click here to access/download
Electronic Supplementary Material
Bbd.png

Fig. Bbe

Fig. Bbf

Click here to access/download
Electronic Supplementary Material
Bbf.png

Fig. Cba

Click here to access/download
Electronic Supplementary Material
Cba.png

Fig. Cbb

Click here to access/download
Electronic Supplementary Material
Cbb.png

Fig. Cbc

Click here to access/download
Electronic Supplementary Material
Cbc.png

Fig. Cbd

Fig. Cbe

Click here to access/download
Electronic Supplementary Material
Cbe.png

Fig. Dba

Fig. Dbb

Click here to access/download

Electronic Supplementary Material

Dbb.png

Fig. Dbd

Click here to access/download
Electronic Supplementary Material
Dbd.png

Fig. Dbe

Fig. Dbf

Click here to access/download
Electronic Supplementary Material
Dbf.png

Fig. Dbg

Fig. Dbh

Click here to access/download
Electronic Supplementary Material
Dbh.png

Fig. Dbc (Fig. 2b)

Fig. Aca

Fig. Acb

Fig. Acc

Fig. Acd

Click here to access/download
Electronic Supplementary Material
Acd.png

Fig. Ace

Fig. Acf

Fig. Bca

Click here to access/download
Electronic Supplementary Material
Bca.png

Fig. Bcb

Click here to access/download
Electronic Supplementary Material
Bcb.png

Fig. Bcc

Click here to access/download
Electronic Supplementary Material
Bcc.png

Fig. Bcd

Click here to access/download
Electronic Supplementary Material
Bcd.png

Fig. Bce

Fig. Bcf (Fig. 3b)

Click here to access/download
Electronic Supplementary Material
Fig. 3b_Bcf.png

Fig. Cca

Click here to access/download
Electronic Supplementary Material
Cca.png

Fig. Ccb

Click here to access/download
Electronic Supplementary Material
Ccb.png

Fig. Ccc

Fig. Ccd

Click here to access/download
Electronic Supplementary Material
Ccd.png

Fig. Cce

Click here to access/download
Electronic Supplementary Material
Cce.png

Fig. Dca

Click here to access/download
Electronic Supplementary Material
Dca.png

Fig. Dcb

Click here to access/download
Electronic Supplementary Material
Dcb.png

Fig. Dcc

Fig. Dcd

Fig. Dce

Fig. Dcf

Fig. Dcg

Fig. Dch